Dynamics of four-wave-mixing oscillators with quasi-phase-matching

Riadh Rebhi, Pierre Mathey,[*] and Hans-Rudolf Jauslin

Institut Carnot de Bourgogne, CNRS–Université de Bourgogne, UMR 5209, 9 Avenue Alain Savary, BP 47870,
21078 Dijon Cedex, France

Gary Cook[†] and Dean R. Evans

Air Force Research Laboratory, Materials and Manufacturing Directorate, Wright-Patterson Air Force Base, Ohio 45433, USA

Daniel Rytz

Forschunginstitute Für Mineralische and Metallische Werkstoffe, Edelsteine/Edelmetalle GmBH, Struhtstrasse 2, Wackenmuhle,
55743 Idar-Oberstein, Germany

Serguey Odoulov

Institute of Physics, National Academy of Sciences, 03 650 Kyiv, Ukraine

The effect of pump-wave misalignment on the oscillation spectra of a semilinear photorefractive oscillator is studied numerically and compared with the results of experiments performed with $BaTiO_3$:Co and $KNbO_3$:Ag,Fe crystals.

PACS number(s): 42.65.Hw, 05.45.−a, 42.65.Sf, 42.70.Nq

I. INTRODUCTION

The single-frequency oscillation in an externally pumped phase-conjugate resonator (also called semilinear photorefractive oscillator with two pumps) [1,2] becomes unstable above a certain critical value of the coupling strength [3]. With the removed degeneracy in frequency the initially static index grating starts to move and this results in an additional nonlinear phase shift of the phase conjugate wave inside the cavity. After two consecutive round trips the nonlinear phase of the oscillation wave does not vanish; moreover it is accumulated with the successive number of round trips in the cavity. To ensure oscillation, this phase shift should either be compensated by any possible means or it should become equal to 2π to restore the in-phase addition of the partial components of the oscillation wave after each double round trip of the cavity [4]. One way to compensate for an undesirable phase shift is to use a frequency shifted feedback [5]. Another way consists of a slight misalignment (of the order of a fraction of milliradian) of the two pump waves [6].

The enhancement of the phase conjugate reflectivity by frequency shift in the case of a perfectly aligned oscillator is independent on the sign of the shift. By the same way, the enhancement of the phase conjugate reflectivity by pump misalignment in the case of a nonfrequency shifted oscillator is independent on the sign of this tilt. Nevertheless if the both effects are considered simultaneously, this symmetry is broken. For misaligned pump waves the calculated beat frequency in the oscillation spectrum for a negative detuning is identical to that for a positive detuning of the same amplitude [6]; the oscillation wave in a cavity with the feedback frequency shifted by arbitrary Ω_M always contains two components, $\Omega_I = +\Omega_M/2$ and $\Omega_{II} = -\Omega_M/2$, which are independent of the sign of the feedback frequency detuning. A sensitivity to the sign of the angular misalignment and to the sign of the feedback frequency shift nevertheless exists and manifests itself in a breaking of the above symmetry when both the pump misalignment and the frequency shifted feedback are imposed simultaneously [7].

In this paper we analyze the combined action of frequency shifted feedback and pump-wave misalignment on the performance of a semilinear photorefractive oscillator, and we compare the experimental results (Sec. II) with the numerical simulations (Sec. III). In Sec. IV a qualitative analysis is presented, which reveals the physical origin of the bifurcations in the oscillation spectra and allows for a prediction of the critical values of the feedback frequency for which a bifurcation may occur for any given set of parameters (pump misalignment angle, pump intensity ratio, coupling strength, etc.). Finally, in Sec. V we discuss the limits of applicability of the considered model and describe the experimental results that are still not explained.

II. EXPERIMENT

A. Experimental procedure

The experiment was performed with a semilinear photorefractive oscillator that involves a coupling of counterpropagating waves and the appearance of reflection index gratings [8]. Figure 1 shows schematically the geometry of the oscillator.

A photorefractive crystal (PRC) is pumped with two nearly counterpropagating waves, labeled 1 and 2 (with intensities $|A_1|^2$ and $|A_2|^2$, respectively). It serves as a nonlinear mirror that can reflect, with amplification, any incident wave 4 (with intensity $|A_4|^2$) which is coherent with pump wave 1. The reflected wave 3 (with intensity $|A_3|^2$) may be nonparal-

———————
*[*]pierre.mathey@u-bourgogne.fr

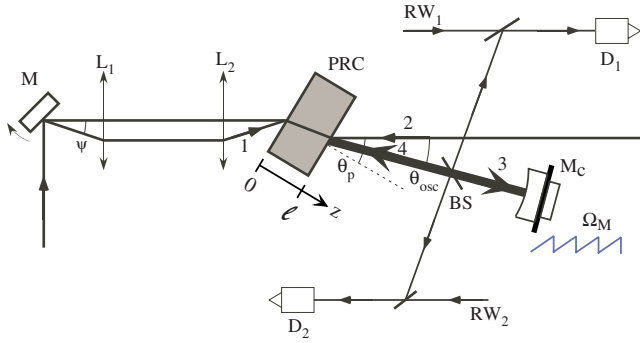[†]Also at Universal Technology Corporation, 1270 N. Fairfield Road, Dayton, Ohio, 45432, USA.

FIG. 1. (Color online) Schematic of the semilinear oscillator with the oscillation waves 3 and 4, waves 1 and 2 that are pumping the photorefractive crystal (PRC), and a conventional cavity mirror M_c mounted on a piezoceramic. D_1 and D_2 are the detectors, RW_1 and RW_2 are the reference waves for heterodyne detection.

lel to the incident wave 4, especially in the case of slightly misaligned pump waves. (For the sake of simplicity we call it, nevertheless, a phase conjugate wave throughout this paper because the misalignment is really rather small, usually below 1 mrad.)

The misalignment is introduced by tilting a mirror M, which is placed in the input focal plane of the symmetric telescope. The lenses L_1 and L_2 with the focal length $F = 8$ cm are separated by $2F$; the tilting mirror and the sample are in the input and output focal planes of the telescope, respectively. In such a way the misalignment angle ψ can be adjusted while keeping the overlap of the two pump waves inside the sample practically unchanged. This is especially important because the two pump waves are loosely focused in the sample with 1 m focal length lenses (not shown in Fig. 1) which are placed at a distance of 90 cm from the crystal.

The oscillator cavity is closed by a conventional mirror M_c mounted on a piezoceramic holder. A saw-tooth voltage is applied to this holder thus ensuring the possibility to control the frequency shift of wave 4 with respect to the frequency of the incident wave 3. A beam splitter (BS) (which is a thin uncoated glass plate) is placed inside the cavity and the reflected beams are collected with detectors D_1 and D_2. With the semitransparent mirrors the reference waves RW_1 and RW_2 with a temporal frequency of the pump waves are sent to the detectors.

Thus the beat frequencies seen by each detector allow for the reconstruction of the spectra of waves 3 and 4. The intensity of wave 4 transmitted through the sample is measured with one more detector which is not shown in Fig. 1. The appearance of the intensity modulation in the signal measured with this detector indicates a bifurcation in the oscillation wave spectrum.

Two photorefractive crystals, Co-doped BaTiO$_3$ ($3.7 \times 4 \times 6.1$ mm^3 along the x, y, and z axes, respectively) or KNbO$_3$ double doped with Fe and Ag [9] ($4 \times 8 \times 7$ mm^3 along the x, y, and z axes, respectively) are used as gain media in the oscillator. Both materials have an enhanced response at high spatial frequencies, i.e., can be used efficiently in a reflection grating geometry of the coherent oscillator [9]. The advantage of KNbO$_3$ is in its faster
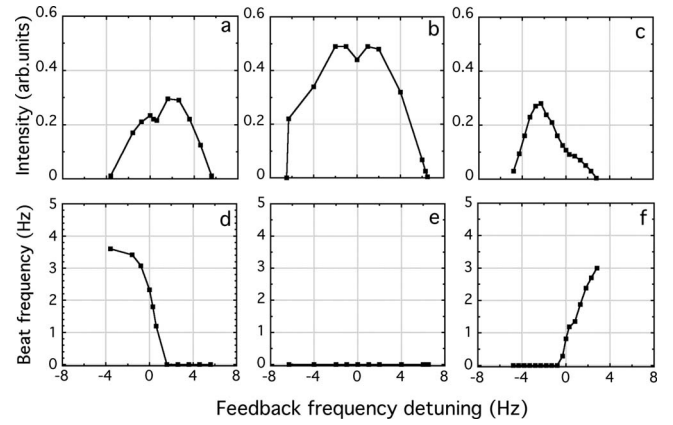

FIG. 2. Experimental dependences of the oscillation intensity [upper row (a)–(c)] and beat frequency [lower row (d)–(f)] on feedback frequency detuning for the oscillator with the KNbO$_3$ crystal. The pump misalignment angle is −0.35, 0, and 0.25 mrad for the [(a) and (d)] left column, [(b) and (e)] central column, and [(c) and (f)] the right column, respectively. The pump ratio is $r = 24$.

response, in the millisecond range for weakly focused beams. The two pump waves are mutually incoherent; they are formed by splitting the Ar$^+$-laser beam ($\lambda = 514.5$ nm), which allows control of the pump ratio in a wide range.

B. Experimental results

In the experiment we measure the oscillation intensity, its beat frequency, and the frequency content of waves 3 and 4 versus, the frequency shift introduced by a piezomirror. We measure these quantities varying the feedback frequency shift Ω_M while holding the other parameters fixed (coupling strength $\gamma\ell$, pump intensity ratio $r = |A_2/A_1|^2$, conventional mirror reflectivity R_c). The Ω_M dependences are measured for different values of the pump misalignment angle ψ. This approach is chosen because the feedback frequency can be adjusted, controlled, and reproduced with high precision, while the measurement of the pump misalignment angle with submilliradian accuracy presents obvious difficulties (because the misalignment in question can be comparable and even much smaller than the divergence of each of the two loosely focused pump beams).

Figure 2 shows the dependences of the oscillation intensity (measured with no reference wave sent to detector $D1$) and the beat frequency on the feedback frequency detuning for nearly perfect alignment (central column) and for positive or negative misalignment of the two pump waves (right and left columns, respectively.) For nearly perfect alignment of the pump waves the oscillation is beat free (no intensity modulation, i.e., zero beat frequency) and the Ω_M dependence of its intensity is nearly bell shaped but with a pronounced dip at zero-frequency detuning.

For misaligned pump waves the single oscillation mode splits into two, with different frequencies, and the output oscillation intensity becomes modulated. Depending on the sign of the misalignment, the beat frequency increases either with the increasing or with the decreasing feedback frequency shift. The point of bifurcation in the frequency spec-
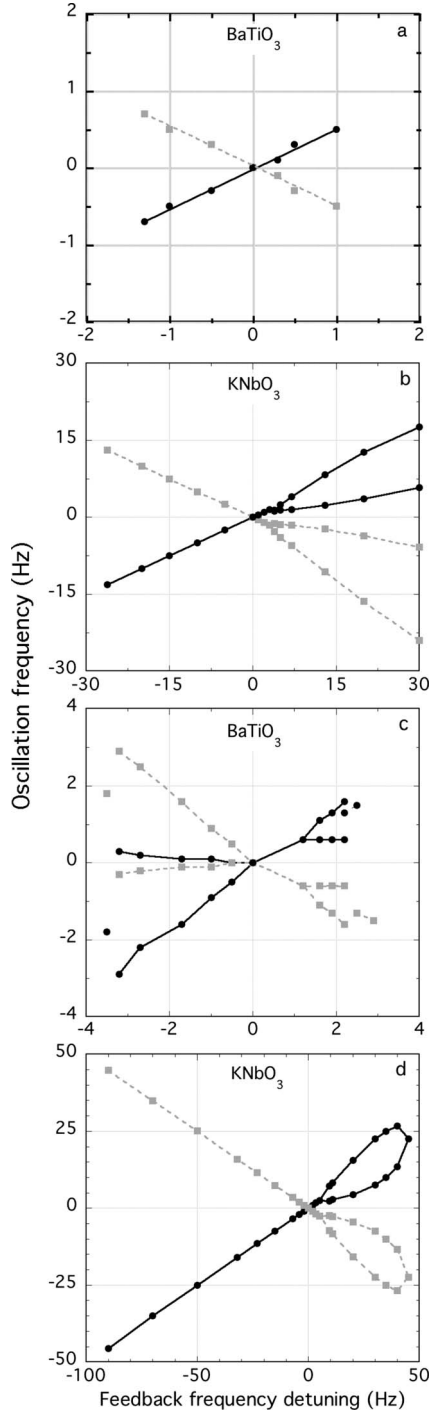
FIG. 3. Experimental dependences of the oscillation frequency versus frequency feedback detuning for different deliberately introduced pump misalignment angles. Data are shown for the oscillator with [(a) and (c)] $BaTiO_3$:Co or [(b) and (d)] $KNbO_3$:Fe,Ag. Black and gray dots mark the frequencies in waves 4 and 3, respectively. Solid lines are shown to guide the eyes. The power of the Ar^+ laser (300 mW) is the same for all the frames in this figure.

trum also marks a singularity in the Ω_M dependence of the oscillation intensity (discontinuity of the derivative $d|A_3|^2/d\Omega_M$).

Several typical dependences of the oscillation frequencies on the feedback frequency detuning are shown in Fig. 3, with

characteristic features that allow them to be distinguished from each other. They can all be obtained with $BaTiO_3$ as well as with $KNbO_3$ crystals. The simplest shape is a linear dependence of the oscillation frequency on the frequency feedback detuning [Fig. 3(a)]. The frequency of wave 3 is Doppler shifted with respect to the frequency of wave 4 by vibrating the conventional mirror

$$\Omega_3 = \Omega_4 + \Omega_M, \tag{1}$$

this is why the dependence shown in Fig. 3(a) looks like a symmetric cross.

Crosslike dependences $\Omega_{osc}=f(\Omega_M)$ are typical for low-loss cavities with large R_c and small threshold values of $\gamma\ell$ in the case of well-aligned pump waves for any pump ratio r. They are also observed for larger $\gamma\ell$ and misaligned pumps provided that the pump intensities are strongly different, i.e., for $r \simeq 100$.

Another representative example of the $\Omega_{osc}=f(\Omega_M)$ dependence is a "fork" shown in Fig. 3(b). Here a single frequency in each oscillation wave, 3 and 4, bifurcates at certain critical values of Ω_M.

Depending on crystal coupling strength and pump misalignment angle, the bifurcation may occur at any Ω_M. The domain of nondegenerate oscillation can include, for example, a region with $\Omega_M=0$. For certain parameter domains a "double-fork" $\Omega_{osc}=f(\Omega_M)$ dependence may appear as shown in Fig. 3(c). The separation between the two critical values of $\Omega_M^{cr}(\text{right})-\Omega_M^{cr}(\text{left})$ can vary considerably and may become negative, i.e., with no beat-free region between two domains of nondegenerate oscillation.

Quite often, with the increase in the feedback frequency, the two-frequency oscillation returns to an oscillation with a single-frequency spectrum, i.e., two symmetric lines in the spectrum exist only within a certain limited range of feedback frequencies. There may be two such Ω_M domains [as shown in Fig. 3(c)] or only one. In the latter case, the $\Omega_{osc}=f(\Omega_M)$ dependence may resemble scissors [Fig. 3(d)].

The bifurcation in the frequency spectrum most often occurs discontinuously, i.e., the two components in the spectrum appear or disappear always with a finite frequency separation between them. Figure 4 shows a typical example for the oscillator with $KNbO_3$ gain medium. The frequency separation at the critical point can be larger or smaller, but we did not observe any case in which it would go smoothly to zero.

The feedback frequency range and the domain of the oscillation frequency detuning depend on the photorefractive sample used; they are much wider for $KNbO_3$ [see Figs. 3(b) and 3(d)] as compared to $BaTiO_3$ [Figs. 3(a) and 3(c)] provided that the total intensity of the pump waves is the same. The frequency detuning of the oscillation wave and the frequency splitting (if it exists) are intensity dependent. They increase roughly linearly with intensity as one can expect for a space-charge decay driven by the dielectric (Maxwell) relaxation time [10].

III. THEORY

A. Equations and procedure

We consider a quasi-phase-matched four-wave-mixing with the wave-vector diagram shown in Fig. 5. For the case
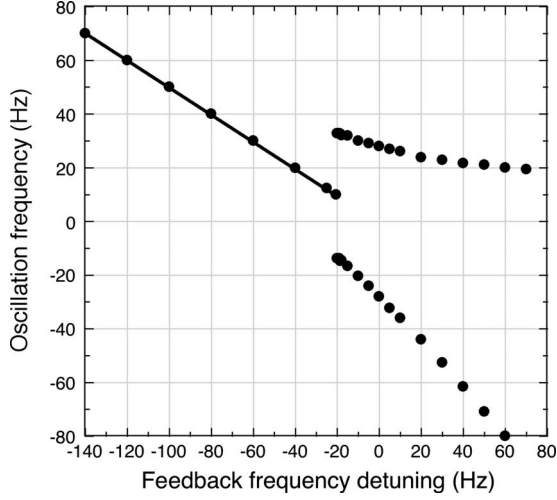
FIG. 4. Zoomed-in feedback frequency dependence of the oscillation spectrum of wave 4 in the vicinity of the critical values of the feedback frequency detuning. The angular detuning is 0.6 mrad.

of reflection gratings the set of equations for the complex amplitudes of the four interacting waves is formulated in a similar way as was done for the transmission gratings [11,12],

$$\frac{\partial A_1}{\partial z} = \nu^* \exp\left(i\frac{\Delta z}{2}\right)A_4, \tag{2}$$

$$\frac{\partial A_2}{\partial z} = \nu \exp\left(i\frac{\Delta z}{2}\right)A_3, \tag{3}$$

$$\frac{\partial A_3}{\partial z} = \nu^* \exp\left(-i\frac{\Delta z}{2}\right)A_2, \tag{4}$$

$$\frac{\partial A_4}{\partial z} = \nu \exp\left(-i\frac{\Delta z}{2}\right)A_1, \tag{5}$$

$$\tau\frac{\partial \nu}{\partial t} + \nu = \frac{\gamma^*}{I_0}\left[A_1^* A_4 \exp\left(i\frac{\Delta z}{2}\right) + A_2 A_3^* \exp\left(-i\frac{\Delta z}{2}\right)\right], \tag{6}$$

where z is the coordinate along the propagation axis, A_i are the complex amplitudes of waves $i=1,2,3,4$, A_i^* are their complex conjugates, $\Delta = k_{1z}+k_{2z}-k_{3z}-k_{4z}$ is a longitudinal component of the wave-vector mismatch, γ is the coupling constant of the photorefractive crystal, ν is the grating am-
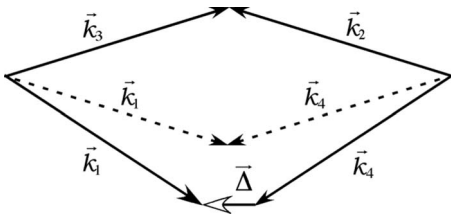

FIG. 5. Phase matching diagram for the considered oscillator with misaligned pump waves.

plitude, I_0 is the total intensity $I_0 = |A_1|^2 + |A_2|^2 + |A_3|^2 + |A_4|^2$, and $\tau \propto 1/I_0$ is the response time of the photorefractive medium that is inversely proportional to the intensity via photoconductivity.

The modified boundary condition for the considered semilinear oscillator takes into account the frequency shift introduced by a piezomirror [5],

$$A_4(z=l,t) = \sqrt{R}A_3(z=l,t)\exp(i\Omega_M t), \tag{7}$$

where R is the intensity reflectivity of the conventional mirror (real) and $\sqrt{R}\exp(i\Omega_M t)$ is an amplitude reflectivity which is complex because of the mirror vibrations.

The numerical simulations of the above equations are performed using the technique described in [13]. A new element consists in the reconstruction of the individual spectra of the oscillation waves 3 and 4. To calculate the frequencies of a particular wave, a reference wave is added with the same frequency as that of the pump waves, and the result is Fourier transformed to get a spectrum.

The results with parameters that are typical for the experimental conditions are presented in the next subsection. We then analyze the threshold conditions and establish the domains of parameters where the splitting in the oscillation spectrum may occur.

B. Results of the simulations

Numerous simulations have been conducted for different coupling strengths $\gamma\ell$, pump ratios r, and dimensionless pump misalignment parameter $\Delta\ell$ (which is defined as the product of the sample thickness ℓ and the longitudinal component of the wave-vector mismatch Δ). To make the analysis easier, the contour plots of the oscillation intensity are constructed in the coordinates $\Delta\ell$ and Ω_M. Then, for some fixed values of the pump misalignment the dependences of the oscillation spectra on the feedback frequency detuning are calculated in order to compare them with the experimental data (such as those shown in Fig. 3).

Figure 6 shows some representative examples of contour plots for increasing coupling strength $\gamma\ell$ for a pump ratio $r=5$ and conventional mirror reflectivity $R_c=0.3$. These values are close to those used in the experiment: first, the selected crystals ensure a high coupling strength that is, however, always smaller than 2π; second, because of cavity losses (Fresnel reflection from uncoated crystal faces, sample absorption, etc.), the effective reflectivity of the conventional cavity mirror is smaller than 100%.

For moderate cavity losses, $R_c \simeq 0.3$, and modest coupling strength, $\gamma\ell = 2-3$, the oscillation is possible only for certain nonzero $\Delta\ell$ and Ω_M and is beat free, i.e., each oscillation wave only has one component in the spectrum [Fig. 6(a)]. With increasing coupling strength the areas of existence of the oscillation increase and for $\gamma\ell = 4$ they merge so that an oscillation becomes possible at $\Delta\ell = 0$ and $\Omega_M = 0$. The largest oscillation intensity is reached, however, still at nonzero values of $\Delta\ell$ and Ω_M. The additional areas appear with an oscillation that has two components in its spectrum [roughly horizontal stripes in Fig. 6(b) filled with gray shading]. The beat frequency here increases with $|\Omega_M|$ within the shown range of feedback frequency detunings.
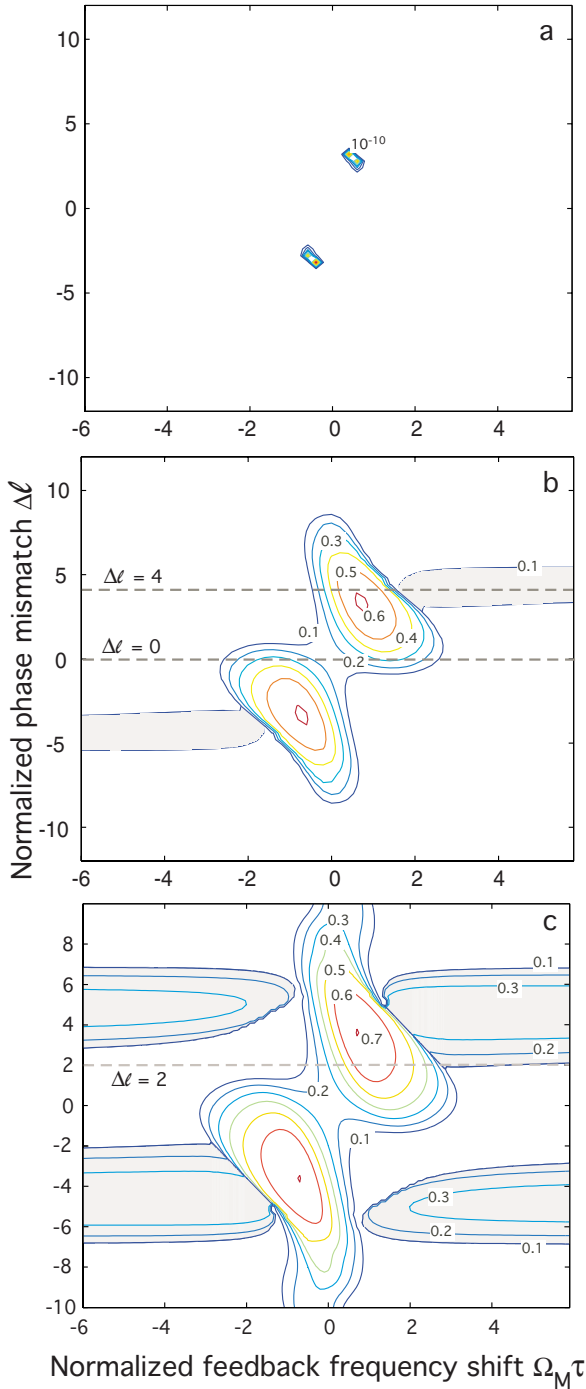
FIG. 6. (Color online) Contour plots of the oscillation intensity as a function of the normalized feedback frequency shift $\Omega_M \tau$ introduced by the vibrating mirror (abscissa) and of the normalized phase mismatch $\Delta \ell$ (ordinate). The pump ratio is $r=5$. The coupling strength $\gamma \ell$ is equal to 2, 4, and 4.5 for (a), (b), and (c), respectively. Areas filled with gray shading correspond to nondegenerate oscillation with two-frequency components. The beat frequency increases with increasing $|\Omega_M|$.

With the coupling strength increasing even more, the domain of existence of the oscillation spreads further and two more stripes with two-frequency spectrum appear [Fig. 6(c)]. At the same time the structure of the central part, with a beat-free oscillation, remains qualitatively the same; the largest intensity is still reached at nonzero $\Delta \ell$ and Ω_M, nearly in the same places where the oscillation appears at small values of the coupling strength.

It should be noted that the window of parameters $\Delta \ell$ and Ω_M chosen for Fig. 6 does not cover all the areas of existence of the oscillation, except for Fig. 6(a). The horizontal stripes in Figs. 6(b) and 6(c) extend, e.g., to infinitely large values of $|\Omega_M|$. Extra "islands" of beat-free oscillation appear for increasing $\Delta \ell$ at large coupling strengths [Fig. 6(c)].

The question may arise as to how the oscillation is possible with a feedback frequency detuning that largely exceeds the reciprocal relaxation time of the photorefractive crystal. One should expect that in the range of $|\Omega_M| \gg 1/\tau$ a photorefractive grating in the sample cannot follow such a quick variation in the phase of the reflected wave 4. The answer is simple; far beyond the bandwidth of the photorefractive gain spectrum, the simulation presented in Fig. 6 describes the so-called mirrorless oscillation that does not need any conventional mirror to appear [1]. Being sent back to the sample by the feedback mirror, it affects nevertheless the oscillation via photoconductivity. It has been shown recently that the threshold of the mirrorless oscillation drops considerably with the misalignment of the pump waves [14]. This is in agreement with the data of Figs. 6(b) and 6(c) where the horizontal stripes are always displaced from $\Delta \ell = 0$.

For relatively modest $|\Omega_M| \simeq 1/\tau$ the contribution of the cavity is important and it strongly modifies the mirrorless oscillation. In the frame of Fig. 6(b), for example, only two horizontal stripes of the two-frequency oscillation are present while for much larger $|\Omega_M|$ the simulations show four stripes that are symmetric with respect to the zero misalignment line $\Delta \ell = 0$. This is due to the fact that two contributions, one from the mirrorless oscillation and the other from the cavity oscillation, add constructively for the stripes visible in Fig. 6(b) and destructively for the two other missing stripes. The asymmetry that has the same origin is also evident in the intensity and in the beat frequency of the four horizontal stripes shown in Fig. 6(c). It should be underlined that this asymmetry disappears for $|\Omega_M| \gg 1/\tau$, where only one of the two contributions (mirrorless oscillation) survives.

From the whole scope of simulations it is possible to find nearly all typical patterns of $\Omega_{osc} = f(\Omega_M)$ dependences that have been observed in the experiment. If in Fig. 6(b) we consider the case of perfectly aligned pump waves, $\Delta \ell = 0$, the oscillation will be beat free everywhere it exists, the dependence $\Omega_{osc} = f(\Omega_M)$ will be crosslike, and the dependence of the oscillation intensity on the feedback frequency will have a dip at $\Omega_M = 0$. This describes qualitatively well the experimental data shown in the central column of Figs. 2 and 3(a).

When considering the normalized misalignment $\Delta \ell = 4$ in Fig. 6(b) we get a forklike $\Omega_{osc} = f(\Omega_M)$ dependence, similar to the experimental findings shown in Fig. 3(b). Finally, for a larger coupling strength, e.g., in Fig. 6(c), one can easily find the range of $\Delta \ell$ in which the behavior should be double-forklike [see Fig. 3(c)].

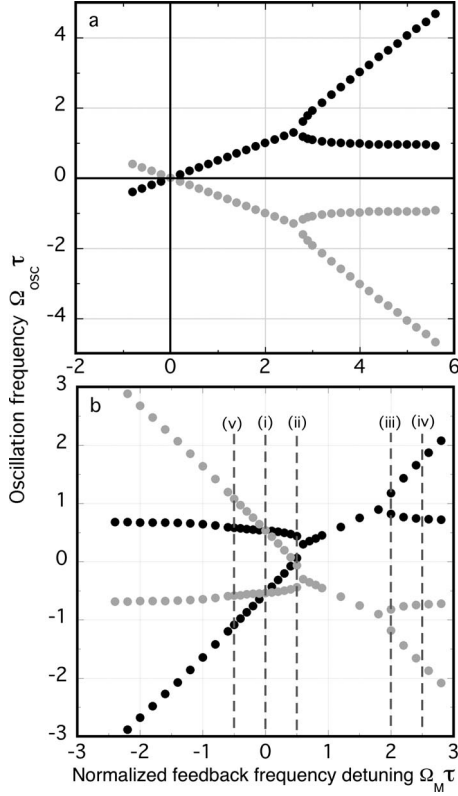To reconstruct the dependence of the oscillation spectra on the feedback frequency detuning, as it was already men-

FIG. 7. Calculated feedback frequency dependences of the oscillation frequencies for (a) $\gamma\ell=4.5$, $r=5$; $\Delta\ell=2.0$, $R_c=0.3$ and (b) $\Delta\ell=2.8$, $R_c=0.1$. Data for waves 3 and 4 are shown in gray and black colors, respectively. Vertical dotted lines relate to Fig. 11.

tioned, the reference wave with the temporal frequency of the pump wave was added to each oscillation wave (3 and 4). The results are shown in Figs. 7(a) and 7(b) for $\Delta\ell=2.0$ and $R_c=0.3$, $\Delta\ell=2.8$ and $R_c=0.1$, respectively, with the coupling strength and the pump ratio being the same, $\gamma\ell=4.5$, r=5. These two dependences resemble qualitatively the experimental observations shown in Figs. 3(b) and 3(c). We did not find, within the frame of the described model, any solutions that give a beat-free oscillation at large feedback frequencies such as the ones shown in the scissorlike spectrum in Fig. 3(d).

A separate task of the simulations was to establish whether the bifurcations in the spectra occur subcritically or supercritically [15,16]. To do so, the same simulations have been performed with more fine discrete steps in the feedback frequency in the vicinity of the critical points in Fig. 7. The results are given in Fig. 8 by open circles for the zoomed-in region of the critical behavior in Fig. 7(a). The discontinuity in the frequency splitting is evident. The same behavior is also detected in the vicinity of the bifurcations in Fig. 7(b).

The data shown in Fig. 7 represent the oscillation frequencies in the established regime. It should be noted that the dynamics of the single-mode oscillation changes qualitatively when approaching a critical point of bifurcation. Being completely smooth far away from the bifurcation, it features damped transient oscillations when approaching the critical value of $\Omega_M\tau$. The closer $\Omega_M\tau$ is to its critical value, the more pronounced these transient oscillations become (Fig. 9).
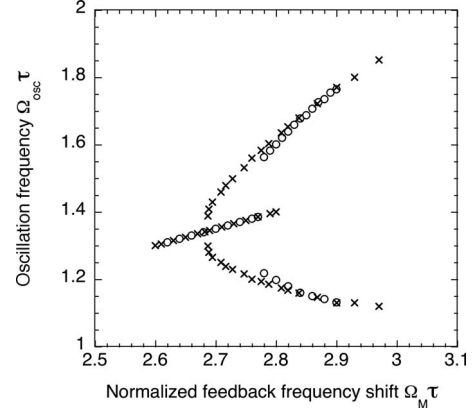

FIG. 8. Calculated feedback frequency dependence of the oscillation spectrum of wave 4 for $\gamma\ell=4.5$, $r=5$, and $\Delta\ell=2.0$ in the vicinity of the critical values of feedback frequency shift in Fig. 7(a). Open circles show the results of the simulations while crosses represent the results of the field self-reproduction analysis described in Sec. IV.

IV. ANALYSIS OF THE FIELD SELF-REPRODUCTION IN THE OSCILLATOR CAVITY

In this section we show how the bifurcations in the oscillation spectra can be predicted from the analysis of the oscillation wave self-reproduction in the cavity. To ensure a stable coherent oscillation two conditions must be met: after each complete round trip of the cavity (1) all losses must be compensated for and (2) the phase of the oscillation wave must return exactly to its initial value (modulo 2π). These conditions are usually called amplitude and phase conditions of oscillation.

For an oscillator with a phase conjugate mirror two round trips are necessary to ensure that the optical field reproduces its initial state [4]. The wave front, the phase, and the frequency detuning of the oscillation wave should return to their initial shape and values. In the nondegenerate case the waves have two components with different frequencies Ω_I and Ω_{II} and the oscillation condition reads,

$$\rho(\Omega_I,\Delta\ell)\rho^*(\Omega_{II},\Delta\ell)R_c = 1, \tag{8}$$

where the reflectivity of the conventional mirror R_c does not depend on small frequency detunings.

This equation follows from the above-described requirement of reproduction of the oscillation field after each double round trip of the cavity. It contains $\rho(\Omega_s,\Delta\ell) = A_4^*(\ell,\Omega_s)/A_3(\ell,\Omega_s)$ which is the amplitude reflectivity of a passive phase conjugate mirror for a fixed $\Delta\ell$ and a particular frequency of the incident signal wave Ω_s.

Equation (8) can be derived rigorously from the stability analysis of the full set of Eqs. (2)–(7). It is obtained in the undepleted pump approximation and corresponds to the oscillation threshold. It also applies for strong wave coupling, provided that ρ is calculated taking into account the pump depletion.

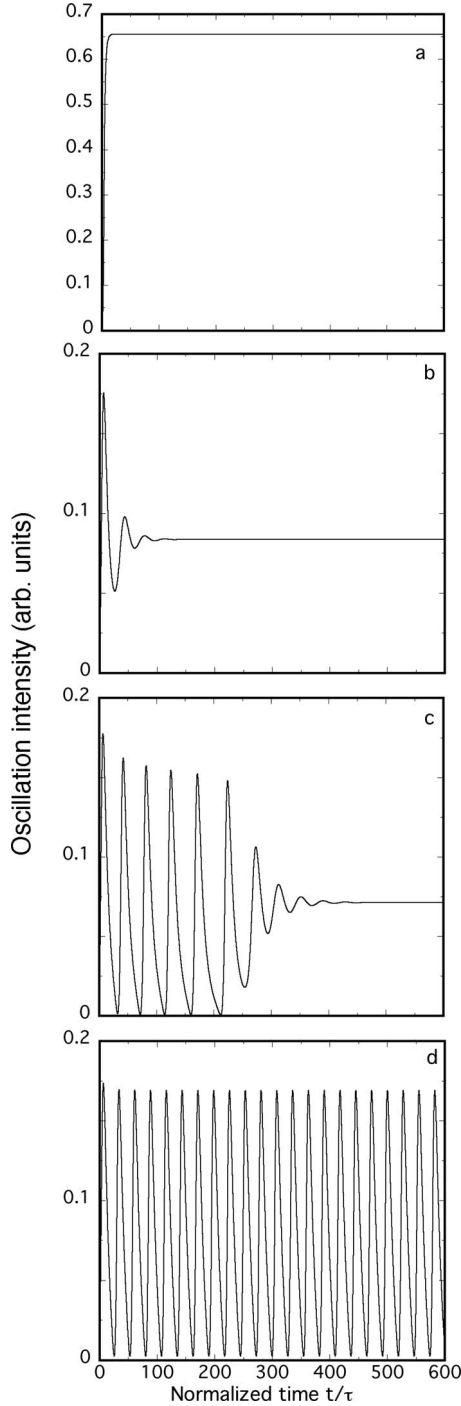The complex equation [Eq. (8)] can be decomposed into two equations,

FIG. 9. Calculated temporal variations in the oscillation intensity for $\gamma\ell = 4.5$, $r = 5$, and $\Delta\ell = 2.0$. The feedback frequency shift is $\Omega_M \tau = 2.7$, 2.75, 2.755, and 2.76 for frames (a), (b), (c), and (d), respectively.

$$|\rho(\Omega_I, \Delta\ell)\rho^*(\Omega_{II}, \Delta\ell)|R_c = 1 \qquad (9)$$

and

$$\arg[\rho(\Omega_I, \Delta\ell)\rho^*(\Omega_{II}, \Delta\ell)] = 2\pi N, \qquad (10)$$

which correspond to the amplitude and phase conditions of oscillation, respectively.

For perfectly aligned pump waves ($\Delta\ell = 0$) and degenerate oscillation ($\Omega_I = \Omega_{II} = 0$) no additional phase shift appears because of phase conjugation such that Eq. (10) is met automatically. The same is true for a nondegenerate single-frequency oscillation, $\Omega_I = \Omega_{II}$ in the case of misaligned pump waves ($\Delta\ell \neq 0$). To satisfy the requirement of Eq. (10) in the general case, the additional phase which is due to the conjugation of the first spectral component should be the same as that which is due to the conjugation of the second spectral component (or they can differ by $2\pi N$).

The above arguments allow for the prediction of the type of oscillation (single frequency, two frequency) expected and determination of the oscillation frequencies from the calculated dependences of $|\rho(\Omega)|^2$ and $\arg[\rho(\Omega)]$. With the analytical expressions for ρ taken, e.g., from [14], we will obtain the frequencies at the oscillation threshold. This is sufficient to establish the type of the oscillation frequency response to the feedback frequency shift (cross, fork, double fork) and to find the approximate location of the bifurcation points. To get the exact values we need to know the strength of the oscillation wave and calculate ρ, taking the signal-to-pump ratio I_4/I_1 equal to 0.06.

Thus, to ensure the threshold conditions for the nondegenerate oscillation it is necessary to find a pair of frequencies, Ω_I and Ω_{II} (if they exist), for which the nonlinear phase that arises when phase conjugation occurs is exactly the same or differs to 2π [i.e., the requirement of Eq. (10) is met]. These frequencies need to belong to a frequency detuning domain with a sufficiently large gain to satisfy also the amplitude condition of oscillation [Eq. (9)].

To prove the validity of this approach, we analyze the frequency response of a passive four-wave-mixing phase conjugator. The dependences of the phase conjugate reflectivity $R_{pc} = |\rho(\Omega_s)|^2$ and the phase of the conjugate beam $\arg[A_4^*(\ell)/A_3(\ell)]$ on the detuning frequency of a signal wave Ω_s have been calculated from the solutions of Eqs. (1) and (5) provided that the signal-to-pump ratio I_4/I_1 is 0.06.

For perfectly aligned pump waves ($\Delta\ell = 0$) these dependences are shown in Figs. 10(a) and 10(b) by gray dotted curves; they are even and odd functions of Ω_s, respectively. No extrema are seen for the dependence of $\arg[A_4^*(\ell)/A_3(\ell)]$ within the frequency range where the reflectivity is greater than unity. Therefore it is impossible to find Ω_I and Ω_{II} for which Eq. (10) can be satisfied; the beat-free oscillation should be observed for arbitrary reflectivity of the conventional mirror and the dependence of the frequencies of waves 3 and 4 on the feedback frequency should be crosslike.

With an increasing misalignment, the above spectra become asymmetric and the range of the $\arg[A_4^*(\ell)/A_3(\ell)]$ variation increases. The simulations show a pronounced minimum in the spectrum of the nonlinear phase already for $\Delta\ell = 1$ so that one necessary condition of the spectrum bifurcation is fulfilled. The phase conjugate reflectivity in the vicinity of this minimum is, however, not large enough to meet the other threshold condition given by Eq. (9).

For a larger misalignment, $\Delta\ell = 2$, the minimum in $\arg[A_4^*(\ell)/A_3(\ell)]$ moves to smaller Ω values and $|\rho|^2$ increases in this frequency domain [black lines in Figs. 10(a) and 10(b)]. As a result, the two threshold conditions [Eqs. (9) and (10)] are met in the vicinity of the minimum of
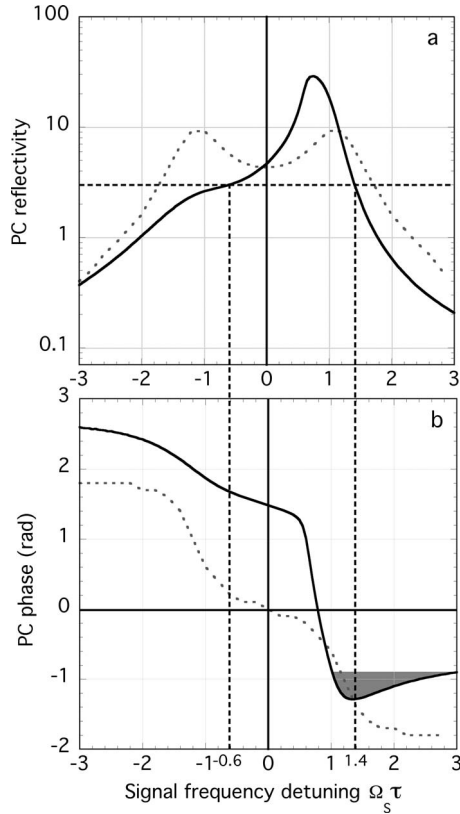
FIG. 10. Calculated dependences of (a) the phase conjugate reflectivity and (b) the nonlinear phase of the phase conjugate wave on frequency detuning of the signal wave for $\gamma\ell=4.5$, $r=5$, and $I_4/I_1=0.06$. $\Delta\ell=0$ and 2 for gray and black curves, respectively.

$\arg[A_4^*(\ell)/A_3(\ell)]$ and the bifurcation of the oscillation frequency should appear.

In Fig. 10(a), a horizontal line marks the level of R_{pc} for which the amplitude condition of oscillation is fulfilled provided that the oscillation is single frequency, i.e., $R_{pc}=(1/R_c)=0.333$. Such an oscillation occurs within the range $-0.58\leq\Omega_{osc}\tau\leq1.42$. This corresponds, for the oscillator, to the feedback frequency detuning $-1.16\leq\Omega_M\tau\leq2.84$ which is in agreement with the results of simulations presented in Figs. 7(a) and 8.

To define the range of a nondegenerate oscillation one should find two oscillation frequencies Ω_I and Ω_{II} for which condition $\sqrt{R_{pc}(\Omega_I)R_{pc}(\Omega_{II})}=1/R_c$ can be met. These frequencies indicate the largest possible interval between two spectral components in the oscillation wave, $\Omega_{II}-\Omega_I$, and largest feedback frequency detuning $\Omega_M^{max}=\Omega_I+\Omega_{II}$ at which the oscillation still exists. The other limit of appearance of nondegenerate oscillation Ω_M^{min} corresponds to the minimum of $\arg[A_4^*(\ell)/A_3(\ell)]$ [see Fig. 10(b)]. From these requirements the range of the nondegenerate oscillation should be $2.66\leq\Omega_M\tau\leq\infty$. Once again, these data are in agreement with those presented in Figs. 7(a) and 8 that follow from the simulation of the oscillation dynamics.

Thus the data in Fig. 10 can be used to reconstruct the dependence of the oscillation frequencies on the feedback frequency shift. The technique consists of the following steps: first we define in Fig. 10(b) different pairs of frequen-
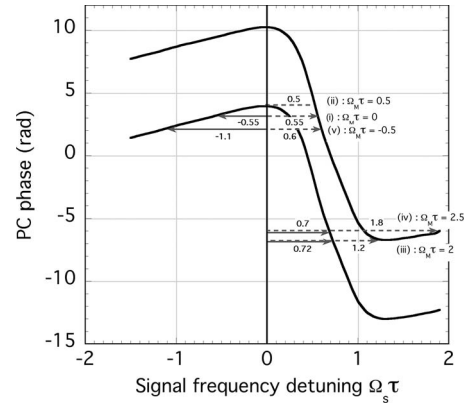

FIG. 11. Calculated dependences of the nonlinear phase in the reflected wave on frequency detuning of the signal wave for $\gamma\ell=4.5$, $r=5$, $\Delta\ell=2.8$, and $I_4/I_1=0.01$. The two branches are shifted in phase by 2π. The horizontal dotted lines are related to the vertical dotted lines in Fig. 7(b).

cies, Ω_I and Ω_{II}, for which the nonlinear phase of the phase conjugate wave is the same; then for each frequency pair we attribute the feedback frequency shift which transforms one frequency into the other, $\Omega_M=\Omega_I+\Omega_{II}$. The data shown in Fig. 8 (crosses) are generated in this way. They practically coincide with the results of the direct simulation above the bifurcation point. They also give a solution below the bifurcation point that does not exist in the simulations.

In fact, within a certain interval of $\Omega_M\tau$ the oscillation conditions are satisfied both for single-frequency and two-frequency oscillations (Fig. 8). In general, the particular oscillation that has a smaller threshold dominates. In nearly all the considered range of $\Omega_M\tau$ the dominant one is the single-frequency oscillation. At the critical value of Ω_M, where the threshold of the two-frequency oscillation becomes smaller, the separation of two oscillation frequencies is already well distinguishable, i.e., the subcritical bifurcation occurs. It is curious that for Ω_M, where two oscillation solutions are allowed, the dynamics show damped oscillations (see Fig. 9). It seems that the oscillator hesitates at first as to which solution it needs to take but finally decides in favor of the single-frequency mode.

Until now we analyzed the cavity oscillation with such set of parameters that its threshold coupling strength is less than that of the mirrorless oscillation [1,14]. With the misalignment increasing to $\Delta\ell=2.8$ the oscillation appears even with no external mirror. It is clear that with the cavity mirror present, the cavity oscillation will be affected by the mirrorless oscillation. For such set of parameters for which the mirrorless oscillation exists, we perform similar simulations of Eqs. (1)–(5) aiming to obtain the signal frequency dependence of $\arg[A_4^*(\ell)/A_3(\ell)]$ and conclude about new possibilities of oscillation frequency bifurcations.

Figure 11 represents the calculated dependence of the nonlinear phase in the phase conjugate wave on the frequency detuning of the signal wave for $\Delta\ell=2.8$ and $I_4/I_1=0.01$. Two extrema appear in Fig. 11 instead of only the one minimum in Fig. 10(b). The second particularity is a much wider range of the nonlinear phase variation in Fig. 11, which exceeds considerably 2π. This leads to consider the

phase condition of oscillation [Eq. (10)] with $N=1$, i.e., taking into account two branches of the solution for $\arg[\rho(\Omega)]$ that differ by 2π.

With this approach we are able to predict the two critical $\Omega_M\tau$ values at which a single-frequency oscillation splits into two frequencies and interpret other particular oscillation spectra such as (1) the nondegenerate oscillation where one frequency is shifted and the other is unshifted with respect to the pump frequency or (2) the nondegenerate oscillation containing identical spectral components in the two oscillation waves 3 and 4. A comparison shows quite good agreement with the data of direct simulations of the oscillation frequencies presented in Fig. 7.

Let us start from a zero feedback frequency shift ($\Omega_M=0$); the data for this particular case are shown in Figs. 7(b) and 11 by (i). By definition, the nondegenerate oscillation should have in this case a symmetric spectrum, with $+\Omega$ and $-\Omega$ components in each of the oscillation waves 3 and 4. This is in agreement with the data of Fig. 7(b) that show identical frequency components for the two oscillation waves (the gray and the black dots coincide). We find in Fig. 11 that the requirement of equal phases for frequency components with the same modulus but different signs is fulfilled for $|\Omega_s|=0.55$, which is in good agreement with the data of Fig. 7(b).

Another particular case corresponds to a nondegenerate oscillation with one component which is not shifted in frequency, $\Omega_I=0$. This situation is depicted as (ii) in Figs. 7(b) and 11. The requirement of equal phases for the two-frequency components, $\Omega_I=0$, $\Omega_{II}=0.5$, is fulfilled as one can see in Fig. 11. This is in agreement with the data of Fig. 7(b).

A slight displacement of the horizontal line (ii) upward brings us to the maximum of the nonlinear phase as a function of the signal frequency. Beyond this critical point the two-frequency oscillation does not exist, i.e., this particular situation corresponds to the point of bifurcation.

In a similar way, the second bifurcation point can be found from the requirement that the horizontal line (iii) in Fig. 11 touches the minimum of the signal frequency dependence of the nonlinear phase. The frequencies $\Omega_I=0.72$ and $\Omega_{II}=1.2$ evaluated at this bifurcation point are also in good agreement with those obtained from simulations [Fig. 7(b)] at $\Omega_M=\Omega_I+\Omega_{II}=1.9$.

It is easy to show that for other values of the frequency detuning Ω_M the results of the direct simulations give values of oscillation frequencies that are very close to those extracted from the threshold analysis. In the vicinity of the minimum we find, in Fig. 11, $\Omega_I=0.7$ and $\Omega_{II}=1.8$, which fit quite well the values extracted from the simulations for $\Omega_M=\Omega_I+\Omega_{II}=2.5$ [case (iv) in the figures]. In the vicinity of the maximum in Fig. 11 we find $\Omega_I=-1.1$ and $\Omega_{II}=0.6$, which also fit well the values extracted from the simulations for $\Omega_M=\Omega_I+\Omega_{II}=-1.5$ [case (v) in the figures]. Thus we conclude that the described analysis can also be applied in the parameter domain where the mirrorless oscillation is allowed.

V. DISCUSSION

In the presented calculations a crucial point for the observation of frequency bifurcation with moderate-gain-factor
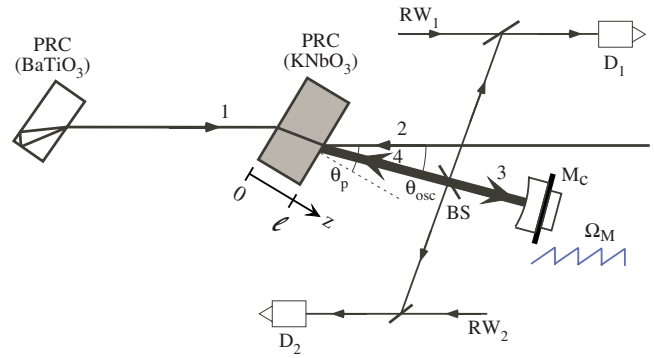

FIG. 12. (Color online) Schematic of the semilinear oscillator with the pump wave 2 generated from the pump wave 1 transmitted through the $KNbO_3$ crystal by a phase conjugation process with the $BaTiO_3$ crystal.

crystals requires a nonzero phase mismatch Δ [see definition after Eq. (6)]. The phase mismatch results in a higher two-beam coupling gain; it decreases both the oscillation threshold and the threshold of the two-frequency oscillation. In our experiment such a mismatch is introduced deliberately by misaligning the two counterpropagating pump waves. In the calculations of Sec. III it is postulated that all four interacting waves are changing their initial propagation directions as compared to the case of $\Delta\ell=0$ [see Eqs. (2)–(5)].

The main scope of the experimental observations fits reasonably well our simulations, so we can conclude that this approximation is quite acceptable. At the same time the question always remains whether this approximation is unique and whether it could be possible to get a phase mismatch without misaligning the two pump waves (by purposely introducing it or simply allowing it to occur naturally).

To answer this question we built the oscillator schematically shown in Fig. 12. This oscillator uses the $KNbO_3$ sample as a gain medium while pump wave 2 is generated by Feinberg's cat phase conjugator [17] that uses a $BaTiO_3$ crystal. In this scheme, pump wave 1 is the phase conjugate replica of pump wave 2 so that the two pump beams are perfectly counterpropagating.

The phase conjugate reflectivity of the cat phase conjugator is measured to be about 30%, but taking into account the Fresnel losses in the $KNbO_3$ crystal we get a pump intensity ratio $r \simeq 10$. The estimated effective reflectivity of the cavity mirror is still $R_c \simeq 0.3$. Keeping the same orientation of the cavity axis and $KNbO_3$ tilt angle we ensure the same coupling strength as in the previous experiments.

Thus the setup depicted in Fig. 12 ensures the best possible alignment of the two pump waves and does not depend on human factors (on the precision of the manual cavity adjustments as in the case of Fig. 1). Also, to give the oscillation waves more freedom in choosing their propagation directions, we do not control the Fresnel number of the cavity (the aperture is removed).

The measured feedback frequency dependence of the oscillation frequencies is shown in Fig. 13. It clearly shows the bifurcation of the oscillation frequency. So, even with perfectly aligned pump waves it is not excluded that the phase
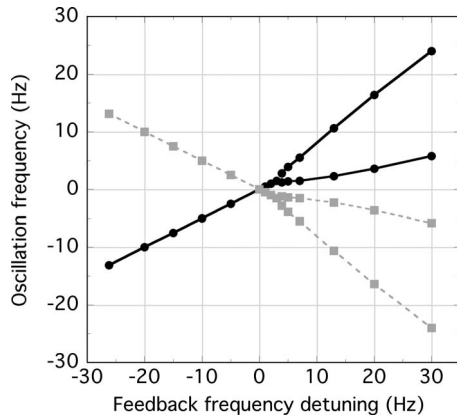
FIG. 13. Feedback frequency dependence of the oscillation frequencies for the oscillator using $KNbO_3$ as a gain medium and $BaTiO_3$ as a phase conjugate mirror that produces pump wave 1 from the transmitted pump wave 2 through the $BaTiO_3$ crystal.

mismatch might appear spontaneously via self-misalignment of different frequency components in the oscillation wave.

VI. CONCLUSIONS

We show in this paper that the oscillation dynamics of the nearly degenerate four-wave-mixing oscillator is very sensi-

tive to even small deviations from the perfect phase matching via misalignments of the two pump waves. An angular detuning of the order of a fraction of milliradian results in a considerable transformation of the oscillation spectrum. The bifurcations in the oscillation spectrum become allowed, whereas a single-frequency oscillation is expected at perfectly aligned pump waves. This conclusion extends to the case of an oscillator with a frequency shifted feedback.

The results of simulations are in reasonable agreement with the main scope of the experimental observations. The simulations show several types of dependence of the oscillation frequencies on the feedback frequency (cross, fork, and double fork) and predict, in agreement with the experimental data, a subcritical type of bifurcation.

It is shown that the type of response of the oscillation spectra to the quasi-phase-matching can also be predicted from the analysis of the frequency dependences of the complex phase conjugate reflectivity. This analysis reveals the domains of multiple solutions for oscillation frequencies, which qualitatively explains the subcritical bifurcation.

[1] A. Yariv and D. Pepper, Opt. Lett. **1**, 16 (1977).

[2] R. K. Jain and G. J. Dunning, Opt. Lett. **7**, 420 (1982).

[3] P. Mathey, S. Odoulov, and D. Rytz, Phys. Rev. Lett. **89**, 053901 (2002).

[4] P. A. Belanger, A. Hardy, and A. Siegman, Appl. Opt. **19**, 479 (1980).

[5] L. P. Yatsenko, B. W. Shore, and K. Bergmann, Opt. Commun. **236**, 183 (2004).

[6] R. Rebhi, P. Mathey, M. Grapinet, H.-R. Jauslin, and S. Odoulov, Appl. Phys. B: Lasers Opt. **91**, 583 (2008).

[7] R. Rebhi, P. Mathey, G. Cook, D. Evans, H. R. Jauslin, and S. Odoulov, Opt. Lett. **34**, 377 (2009).

[8] M. Grapinet, P. Mathey, S. Odoulov, and D. Rytz, Appl. Phys. B: Lasers Opt. **77**, 551 (2003).

[9] D. R. Evans, G. Cook, J. L. Carns, M. A. Saleh, S. A. Basun, J. M. Seim, and G. J. Mizell, Opt. Lett. **31**, 89 (2006).

[10] L. Solymar, D. J. Webb, and A. Grunnet-Jepsen, *The Physics and Applications of Photorefractive Materials* (Clarendon Press, Oxford, 1996).

[11] N. V. Kukhtarev, T. I. Semenets, K. H. Ringhofer, and G. Tomberger, Appl. Phys. B: Lasers Opt. **41**, 259 (1986).

[12] C. Denz, J. Goltz, and T. Tschudi, Opt. Commun. **72**, 129 (1989).

[13] M. Grapinet, P. Mathey, H. R. Jauslin, B. Sturman, D. Rytz, and S. Odoulov, Eur. Phys. J. D **41**, 363 (2007).

[14] R. Rebhi, P. Mathey, H.-R. Jauslin, and B. Sturman, Opt. Lett. **33**, 2773 (2008).

[15] M. C. Cross and P. C. Hohenberg, Rev. Mod. Phys. **65**, 851 (1993).

[16] R. Kubo, *Statistical Mechanics* (North-Holland, Amsterdam, 1965).

[17] J. Feinberg, Opt. Lett. **7**, 486 (1982).